## Supplementary Information

**A R-loop sensing pathway mediates the relocation of transcribed genes to nuclear pore complexes**

Arianna Penzo, Marion Dubarry, Clémentine Brocas, Myriam Zheng, Raphaël M. Mangione, Mathieu Rougemaille, Coralie Goncalves, Ophélie Lautier, Domenico Libri, Marie-Noëlle Simon, Vincent Géli, Karine Dubrana & Benoit Palancade

Includes:

**Supplementary Figures 1-5**

**Supplementary Tables 1-4**

**Supplementary References**

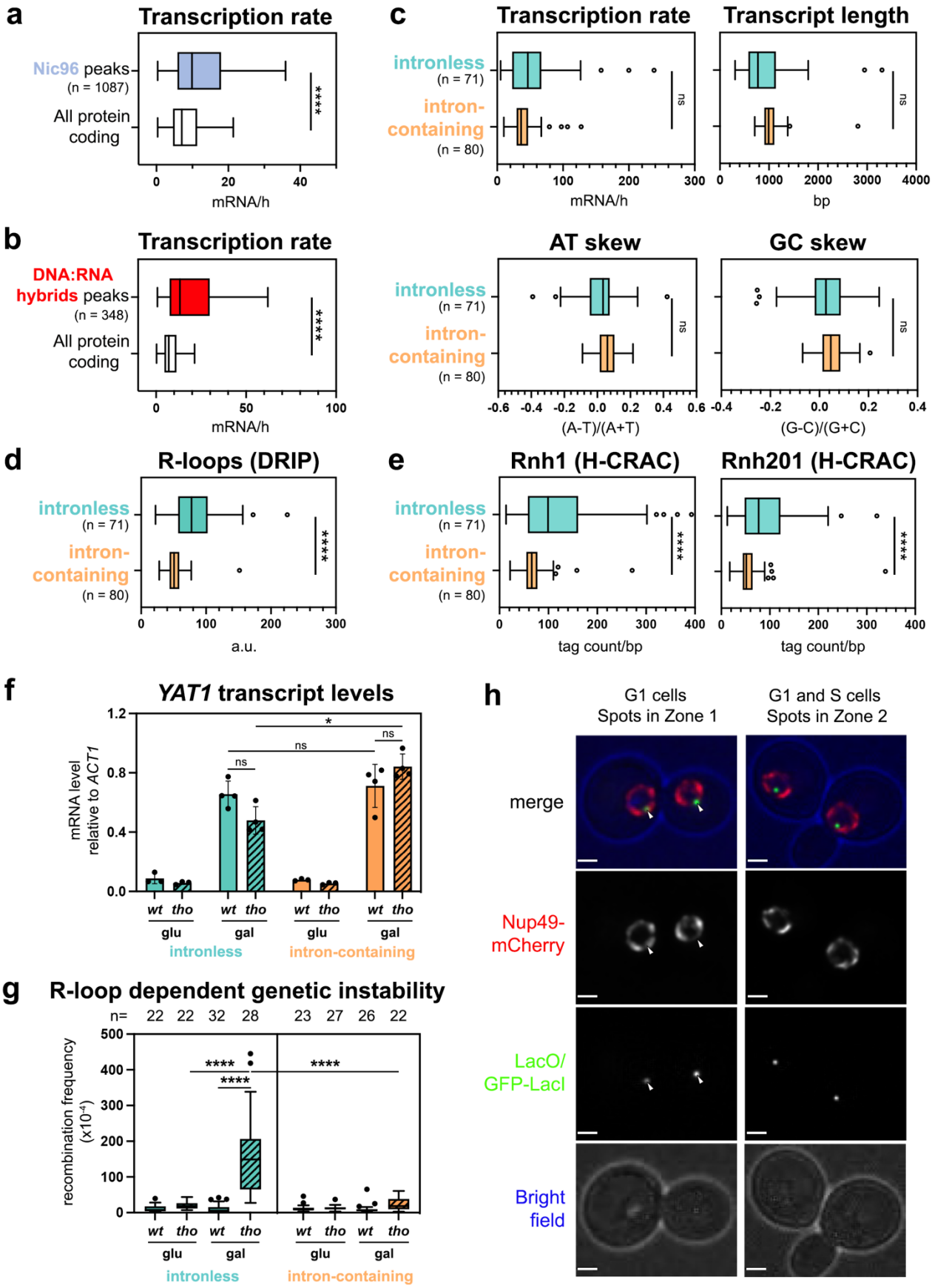


**Supplementary Figure 1. Validation of the gene datasets and reporter systems used to analyze the relationships between NPC association and R-loop levels.** See legend on next page.

**Supplementary Figure 1. Validation of the gene datasets and reporter systems used to analyze the relationships between NPC association and R-loop levels. a-b,** Transcription rates (mRNA/hr)[1] for the genes associated with Nic96 peaks (this study), DNA:RNA hybrid peaks [2] or all protein-coding genes. The number of considered peaks is indicated. Outliers identified according to Tukey's definition are not represented on this scale but have been included in statistical analyses. Statistical test: two-sided Mann-Whitney-Wilcoxon test; ****, $p<10^{-4}$. **c,** Transcription rates (mRNA/hr)[1], transcript length (pre-mRNA, bp), AT-skew and GC-skew for the intronless and intron-containing highly-expressed genes as previously defined[3] (listed in Supplementary Table 1). Statistical test: two-sided Mann-Whitney-Wilcoxon test**. d-e,** R-loops levels for the same groups of intronless and intron-containing highly-expressed genes as scored by DNA:RNA hybrid immunoprecipitation (DRIP[2]; **d**), RNase H1 CRAC[4] (**e**, left panel) and RNase H2 CRAC[4] (**e**, right panel). Statistical test: two-sided Mann-Whitney-Wilcoxon test; ****, $p<10^{-4}$. **f,** qPCR-based quantification of *YAT1* mRNA levels from *wt* or *tho* (*mft1*Δ) mutant cells grown in glycerol-lactate medium and further treated with either glucose (glu) or galactose (gal) for 5h (values normalized to *ACT1* RNA levels and relative to *wt*; mean±SD, n=3 independent experiments in glucose, 4 in galactose). Statistical test: two-sided Mann-Whitney-Wilcoxon test; *, $p=2.86 \times 10^{-2}$. **g,** Recombination frequencies (fraction of Leu+ prototrophs, $\times 10^{-4}$; n refers to the number of biologically independent cultures assessed for each strain/condition) were calculated as described in Methods for *wt* or *tho* (*mft1*Δ) mutant cells carrying *YAT1* transgenes, grown in glycerol-lactate medium and further treated with either glucose (glu) or galactose (gal) for 5h. Boxes extend from the 25th to 75th percentiles, with the median displayed as a line. The whiskers mark the minimum and maximum, displaying as individual points the values that fall outside of 1.5 time the inter-quartile range of the first or third quartile (Tukey's definition). Statistical test: two-sided Mann-Whitney-Wilcoxon test; ****, $p<10^{-4}$. **h,** Single channel images illustrating the principle of the zoning assay (*YAT1* tagged locus, Fig. 1g-h). Arrowheads point to loci localized in zone 1, and thus scored as peripheral. Note their colocalization with the Nup49-mCherry signal, even if not within the most prominent NPC patches. Scale bar = 1µm. Source data are provided as a Source Data file.

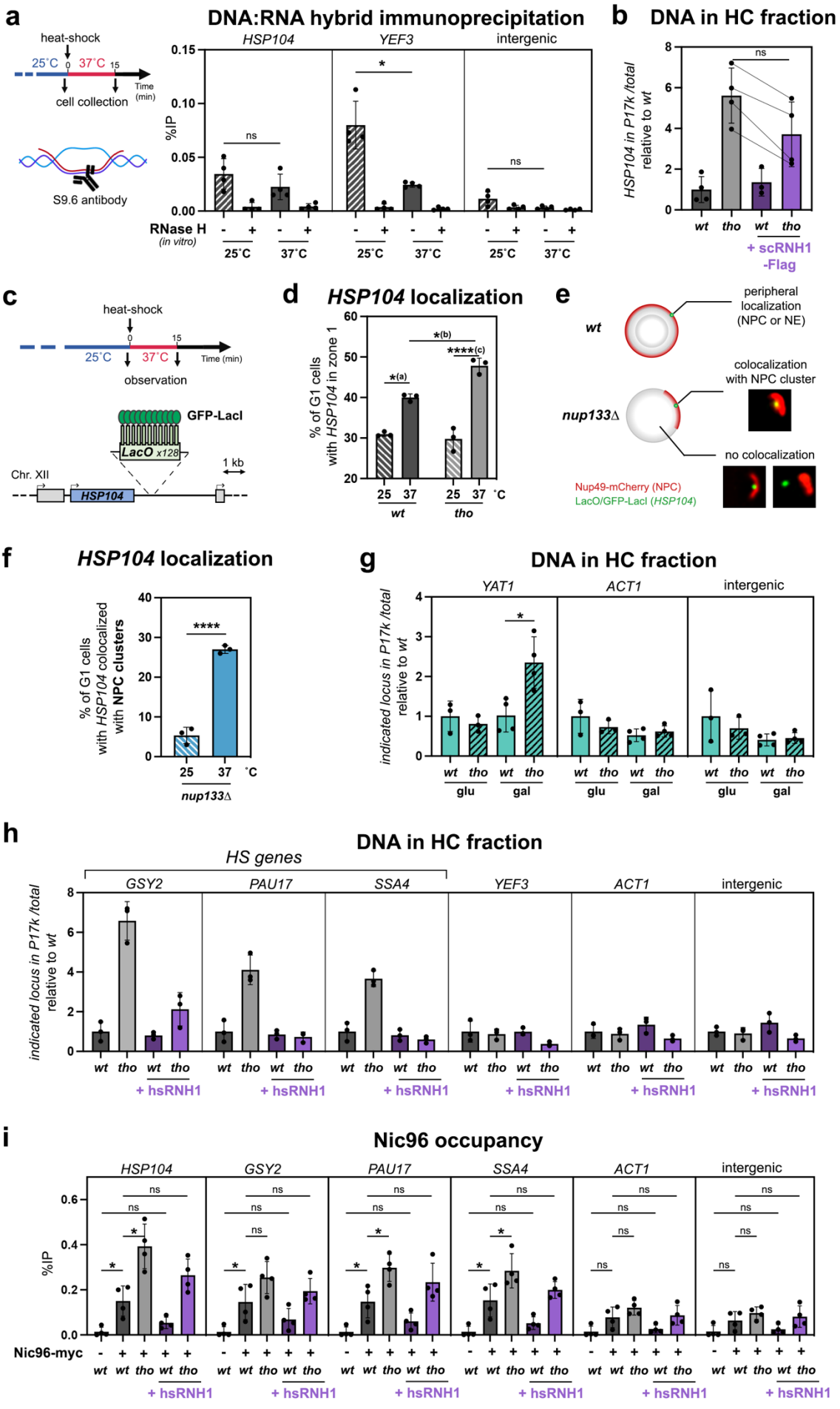


**Supplementary Figure 2. Characterization of R-loop formation and relocation for heat shock loci.** See legend on next page.

**Supplementary Figure 2. Characterization of R-loop formation and relocation for heat shock loci. a,** left panel, time-line of the heat shock and cell collection procedure used for DNA:RNA hybrid immunoprecipitation (DRIP) experiments. Right panel, DNA:RNA hybrid detection by DRIP-qPCR in *wt* cells grown at 25°C or heat-shocked at 37°C for 15min (% of IP; n=4 independent experiments). When indicated, DNA extracts were treated with RNase H *in vitro* prior to immunoprecipitation. Statistical test: two-sided Mann-Whitney-Wilcoxon test; *, p=2.86 x $10^{-2}$. **b**, qPCR-based quantification of the amount of DNA from the indicated loci in heavy chromatin (HC) fractions from *wt* or *tho* (*mft1*Δ) mutant cells transformed with either an empty vector or the *tetOFF-scRNH1-Flag* construct (+scRNH1), and heat-shocked at 37°C for 15min (% of the indicated locus in P17K relative to total [S17K+P17K]; mean±SD, n=4 independent experiments or 3 for wt+scRNH1, relative to *wt*). Statistical test: two-sided Mann-Whitney-Wilcoxon test. **c**, Schematic representation of the time-line of the procedure and of the tagged genomic *HSP104* locus used for microscopy experiments. **d,** Fraction of G1 cells (%) showing *HSP104* in zone 1 (mean±SD, n=3 independent experiments), in the indicated strains grown at 25°C or heat shocked at 37°C for 15min. Statistical test: two-sided Fisher's exact test; P-values were calculated on the total number of counted cells (between 326 and 409 cells/condition); (a), p=1.59 x $10^{-2}$; (b), p=2.45 x $10^{-2}$; (c), p=4.96 x $10^{-7}$. Values are the same as in Fig. 3h. **e**, Representative images of the position of the tagged genomic *HSP104* locus (in green) in *nup133*Δ cells with respect to NPC clusters (visualized owing to the expression of the Nup49-mCherry nucleoporin). **f,** Fraction of G1 cells (%) showing colocalization of *HSP104* with the NPC clusters in *nup133*Δ cells grown at 25°C or heat-shocked at 37°C for 15min (mean±SD, n=3 independent experiments). Statistical test: two-sided Fisher's exact test; the P-value was calculated on the total number of counted cells (25°C: 100; 37°C: 112); ****, p=3.27 x $10^{-5}$. **g**, qPCR-based quantification of the amount of DNA from the indicated loci in heavy chromatin (HC) fractions from *GAL-YAT1* cells, either *wt* or *tho* (*mft1*Δ), grown in glycerol-lactate medium and further treated with either glucose (glu) or galactose (gal) for 5h (% of the indicated locus in P17K relative to total [S17K+P17K]; mean±SD, n=3 independent experiments in glucose or 4 in galactose, relative to *wt*). Statistical test: two-sided Mann-Whitney-Wilcoxon test; *, p=2.86 x $10^{-2}$. Note that the co-fractionation phenotype is less pronounced for *YAT1* than for the HS genes, possibly in line with the particular high-frequency promoter firing in the latter case[5]. **h**, qPCR-based quantification of the amount of DNA from the indicated loci in heavy chromatin (HC) fractions from *wt* or *tho* (*mft1*Δ) mutant cells transformed with either an empty vector or the *GPD-hsRNH1* construct (+hsRNH1), and heat-shocked at 37°C for 15min (% of the indicated locus in P17K relative to total [S17K+P17K]; mean±SD, n=3 independent experiments, relative to *wt*). **i,** Nic96-myc enrichment was analyzed at the indicated loci by ChIP-qPCR in *wt* or *tho* (*mft1*Δ) mutant cells transformed with either an empty vector or the *GPD-hsRNH1* construct (+hsRNH1), and heat shocked at 37°C for 15min (% of immunoprecipitation; mean±SD, n=4 independent experiments). A strain expressing an untagged version of Nic96 (Nic96-myc: -) was used as a control. Statistical test: two-sided Mann-Whitney-Wilcoxon test; *, p=2.86 x $10^{-2}$. Note that Nic96 ChIP signals observed over control or intergenic loci vary slightly in conditions of altered R-loop levels, albeit in a non-significant manner, likely reflecting their proximity with one of the multiple NPC contact sites scored in our ChIP-seq analysis (more than 1000 peaks over the genome, Fig. 2e). Source data are provided as a Source Data file.

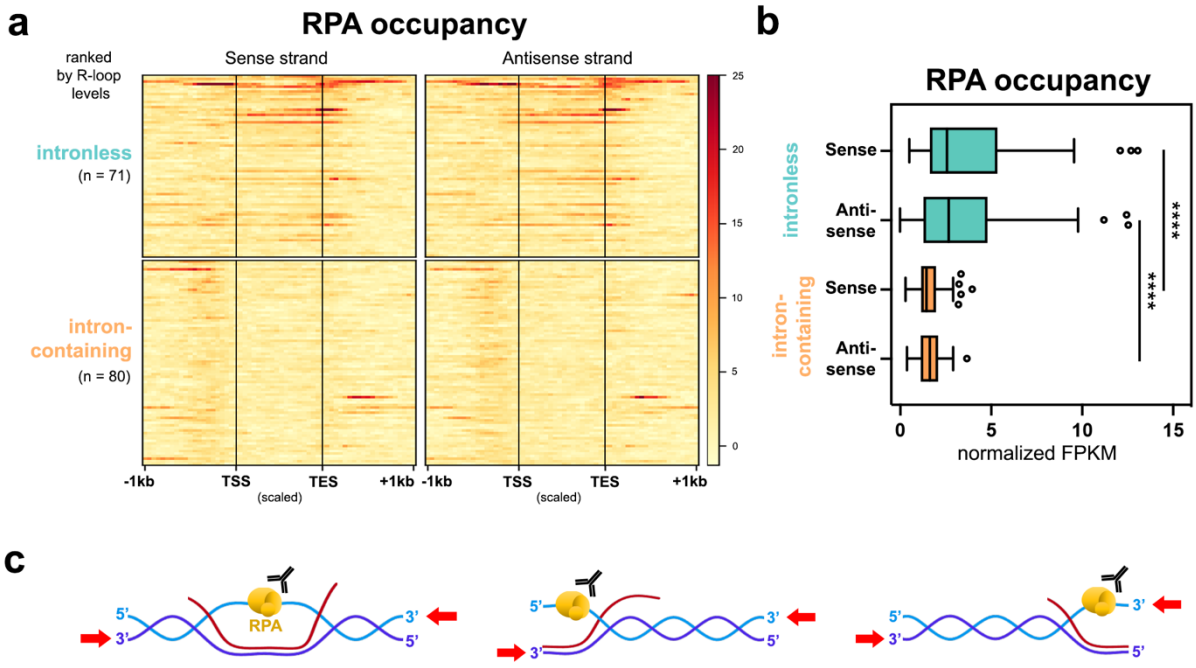


**Supplementary Figure 3. Characterization of the R-loop gating pathway. a,** Heatmap analysis of RPA occupancy at the sense or antisense strand of highly-transcribed intronless and intron-containing genes, aligned at their Transcription Start Site (TSS) and Transcription End Site (TES), in *wt* cells arrested in G1 (strand-specific RPA ChIP-seq dataset)[6]. Only the regions between the TSS and the TES are scaled. Genes are grouped based on their intron content and ranked according to their R-loop levels (from Fig. 1c). Note that the position of RPA tracks does not perfectly correlate with the localization of R-loops (Fig. 1c), raising the possibility that RPA could also associate to genomic loci in G1, independently of R-loop formation. **b,** Average RPA occupancy at the sense or antisense strand of highly-transcribed intronless and intron-containing genes (normalized to input DNA). Statistical test: two-sided Mann-Whitney-Wilcoxon test; ****, $p<10^{-4}$. **c,** Immunoprecipitation of R-loop-bound RPA is not expected to retrieve directional signals in strand-specific ChIP-seq. In the procedure used[6], immunoprecipitated DNA is denatured and 3'-specific adaptors are ligated (red arrows) prior to library amplification. Since R-loops are expected to be smaller (≈150bps)[7] than sonicated DNA fragments (200-500bp), this treatment will similarly tail both strands with the adaptors. Source data are provided as a Source Data file.

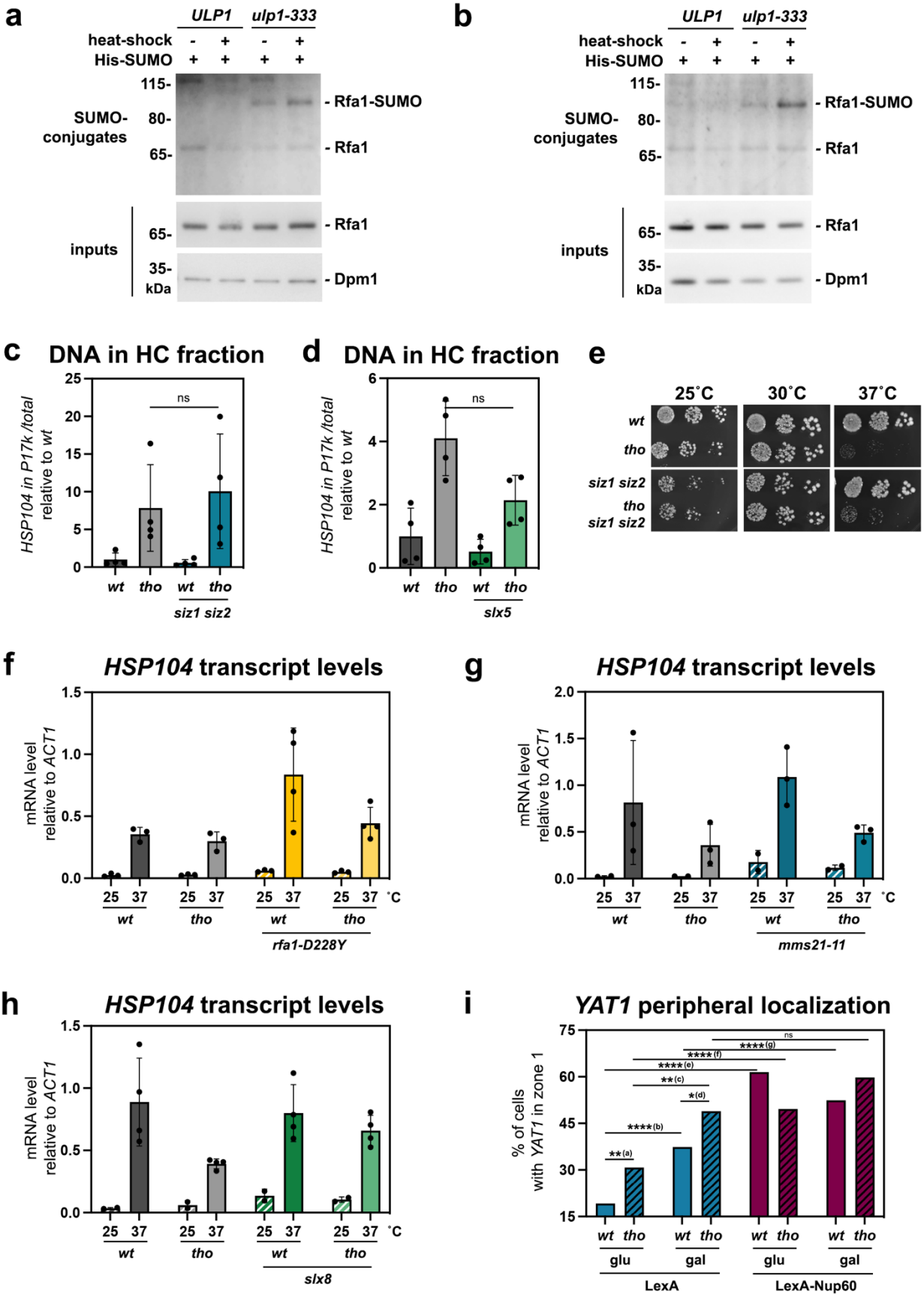


**Supplementary Figure 4. Control experiments related to SUMOylation, fractionation, growth and tethering assays.** See legend on next page.

**Supplementary Figure 4. Control experiments related to SUMOylation, fractionation, growth and tethering assays. a-b,** biological replicates of the SUMOylation assay featured in Fig. 4a. Rfa1 is detected by western-blot in input fractions (bottom panel) or purified SUMO-conjugates (top panel) obtained from the indicated strains. Wild type (*ULP1*) or *ulp1-333* cells carrying the His-SMT3 (His-SUMO) construct were grown at 25°C or heat shocked at 37°C for 15min (heat-shock). The positions of unmodified and mono-SUMOylated Rfa1 are indicated, as well as molecular weights (kDa, kilodaltons). Dpm1 serves as a loading control. **c-d**, qPCR-based quantification of the amount of DNA from the indicated loci in heavy chromatin (HC) fractions from the indicated strains heat-shocked at 37°C for 15min (% of *HSP104* in P17K relative to total [S17K+P17K]; mean±SD, n=4 independent experiments, relative to *wt*). Statistical test: two-sided Mann-Whitney-Wilcoxon test. **e,** Serial dilutions of the indicated strains were grown at the indicated temperatures on rich medium (YPD). **f-h,** qPCR-based quantification of *HSP104* mRNA levels from the indicated strains grown at 25°C or heat-shocked at 37°C for 15min (values normalised to *ACT1* RNA levels and relative to *wt*; mean±SD, n=2-3 independent experiments for 25°C and 3-4 for 37°C). **i,** Fraction of cells (%) showing intronless *YAT1* in zone 1, in *wt* or *tho* (*mft1*Δ) mutant cells carrying either LexA- or LexA-Nup60-expressing constructs, grown in glycerol-lactate medium and further treated with glucose or galactose for 5h. Statistical test: two-sided Fisher's exact test; P-values were calculated on the total number of counted cells (between 141 and 270 cells/condition); (a), $p=8.22 \times 10^{-3}$; (b), $p=7.24 \times 10^{-6}$; (c), $p=1.34 \times 10^{-3}$; (d), $p=2.43 \times 10^{-2}$; (e), $p<10^{-8}$; (f), $p=2.18 \times 10^{-4}$; (g), $p=5.95 \times 10^{-4}$. Source data are provided as a Source Data file.

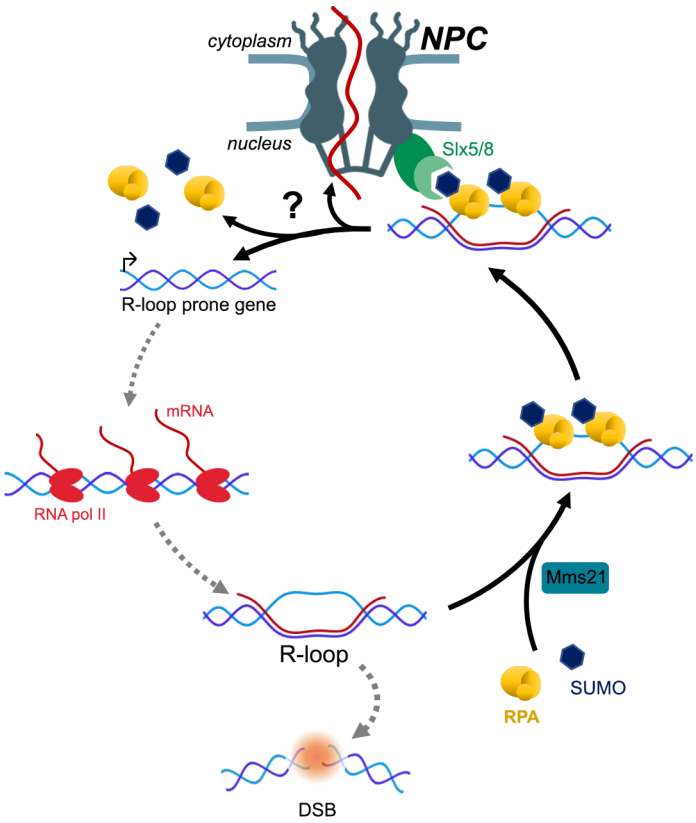


**Supplementary Figure 5. Proposed model for the relocation of R-loop forming loci to nuclear pore complexes.**

**Supplementary Table 1. Intronless and intron-containing highly-expressed genes considered in this study**.

**Intronless (n=71)**

| Systematic Name | Standard Name | Systematic Name | Standard Name |
|---|---|---|---|
| YLR029C | RPL15A | YGR192C | TDH3 |
| YLR110C | CCW12 | YDR276C | PMP3 |
| YJL158C | CIS3 | YDR033W | MRH1 |
| YLR044C | PDC1 | YIL053W | GPP1 |
| YKL060C | FBA1 | YML028W | TSA1 |
| YKL152C | GPM1 | YHR193C | EGD2 |
| YGL008C | PMA1 | YNL031C | HHT2 |
| YEL027W | VMA3 | YDL055C | PSA1 |
| YNL145W | MFA2 | YJR009C | TDH2 |
| YLR249W | YEF3 | YGR234W | YHB1 |
| YCR012W | PGK1 | YEL009C | GCN4 |
| YLR075W | RPL10 | YLR441C | RPS1A |
| YDR382W | RPP2B | YBL003C | HTA2 |
| YKL056C | TMA19 | YGL147C | RPL9A |
| YOR063W | RPL3 | YJL190C | RPS22A |
| YPL131W | RPL5 | YBR010W | HHT1 |
| YAL038W | CDC19 | YDR134C | CCW22 |
| YJR123W | RPS5 | YDR225W | HTA1 |
| YHL015W | RPS20 | YDR418W | RPL12B |
| YOL086C | ADH1 | YGL253W | HXK2 |
| YOL040C | RPS15 | YKL216W | URA1 |
| YDR050C | TPI1 | YLR300W | EXG1 |
| YDR224C | HTB1 | YLL045C | RPL8B |
| YGL123W | RPS2 | YNL030W | HHF2 |
| YDR461W | MFA1 | YDR155C | CPR1 |
| YOR369C | RPS12 | YNL067W | RPL9B |
| YLR167W | RPS31 | YLR264W | RPS28B |
| YDL081C | RPP1A | YDL192W | ARF1 |
| YLR340W | RPP0 | YEL054C | RPL12A |
| YOR167C | RPS28A | YGR037C | ACB1 |
| YNL178W | RPS3 | YPL037C | EGD1 |
| YOL039W | RPP2A | YHR089C | GAR1 |
| YOL109W | ZEO1 | YDL014W | NOP1 |
| YHR174W | ENO2 | YEL034W | HYP2 |
| YGR060W | ERG25 | YBR106W | SND3 |
| YLR325C | RPL38 | | |

**Intron-containing (n=80)**

| Systematic Name | Standard Name | Systematic Name | Standard Name |
|---|---|---|---|
| YGR034W | RPL26B | YHL001W | RPL14B |
| YLR061W | RPL22A | YNL302C | RPS19B |
| YAL003W | EFB1 | YOR182C | RPS30B |
| YBL092W | RPL32 | YIL133C | RPL16A |
| YGL103W | RPL28 | YPR132W | RPS23B |
| YNL112W | DBP2 | YPL143W | RPL33A |
| YGL030W | RPL30 | YML026C | RPS18B |
| YDL130W | RPP1B | YML024W | RPS17A |
| YLR048W | RPS0B | YDL083C | RPS16B |
| YJL189W | RPL39 | YLR388W | RPS29A |
| YPR043W | RPL43A | YIL148W | RPL40A |
| YBR048W | RPS11B | YJL177W | RPL17B |
| YOL127W | RPL25 | YNL162W | RPL42A |
| YHR010W | RPL27A | YOL120C | RPL18A |
| YDL061C | RPS29B | YLR406C | RPL31B |
| YIL069C | RPS24B | YIL052C | RPL34B |
| YMR116C | ASC1 | YOR096W | RPS7A |
| YHR021C | RPS27B | YDR447C | RPS17B |
| YGL031C | RPL24A | YLR185W | RPL37A |
| YDL075W | RPL31A | YLR333C | RPS25B |
| YML073C | RPL6A | YKR094C | RPL40B |
| YNL069C | RPL16B | YDR064W | RPS13 |
| YIL018W | RPL2B | YDL082W | RPL13A |
| YJR145C | RPS4A | YDR471W | RPL27B |
| YDR500C | RPL37B | YDR025W | RPS11A |
| YKR057W | RPS21A | YLR448W | RPL6B |
| YBL087C | RPL23A | YBR189W | RPS9B |
| YGL189C | RPS26A | YOR312C | RPL20B |
| YBR191W | RPL21A | YKL156W | RPS27A |
| YPL079W | RPL21B | YNL301C | RPL18B |
| YGR118W | RPS23A | YCR031C | RPS14A |
| YGR148C | RPL24B | YMR143W | RPS16A |
| YJL136C | RPS21B | YBL027W | RPL19B |
| YOR234C | RPL33B | YHR141C | RPL42B |
| YHR203C | RPS4B | YER074W | RPS24A |
| YER117W | RPL23B | YGR214W | RPS0A |
| YKL180W | RPL17A | YNL096C | RPS7B |
| YOR293W | RPS10A | YMR142C | RPL13B |
| YDR450W | RPS18A | YLR344W | RPL26A |
| YOL121C | RPS19A | YMR230W | RPS10B |

**Supplementary Table 2. Strains used in this study**.

| CODE | NAME | GENOTYPE | USAGE (Fig.) | SOURCE |
|---|---|---|---|---|
| YBP539 | *wt* (BY4742) | MATalpha *ura3 his3 leu2 lys2* | Fig. 1b-d, 2a-e, S2a-b, S2h-i, 3c, 4g, S4c-f, S4h, 5a | Euroscarf |
| YBP936 | *wt* (BY4741) | MATa *ura3 his3 leu2 met15* | Fig. 3d | Euroscarf |
| YBP1525 | *wt* (W303) | MATalpha *ade2 ura3 his3 trp1 leu2 can1* | Fig. 3b, 4a, 4d-f, S4a-b, S4g, 5a | Gift from C. Dargemont. |
| FSY3523 | *wt* (*HSP104*) | (W303) *LacO@HSP104 3'::TRP1 ade2-1::GFP-LacI-ADE2 NUP49-GFP* | strain construction | Rougemaille et al.[8] |
| YKD2204 | *wt* (*HSP104)* | (W303) *LacO@HSP104 3'::TRP1 ade2-1::GFP-LacI-ADE2 pRS316-NUP49-mCherry* | Fig. S2d, 3h, 4c | Derived from FSY3523 through crosses. |
| FSY5216 | *wt* (*GAL10*) | (W303) *LacO@GAL10 3'::TRP1 his3::LacI-GFP::HIS3 LexA-BS@GAL1 3' NUP49-GFP + pBTM116-URAr-LexA* | strain construction | Texari et al.[9] |
| YKD1683 | *wt* (*GAL10*) | (W303) *LacO@GAL10 3'::TRP1 his3::LacI-GFP::HIS3 LexA-BS@GAL1 3' NUP49::NUP49-mCherry-HphMX* | strain construction | Derived from FSY5216 through crosses. |
| YPB2102 | *wt* (*YAT1)* | (W303) *LacO@GAL10 3'::TRP1 his3::LacI-GFP::HIS3 LexA-BS@GAL1 3' NUP49::NUP49-mCherry-HphMX leu2Δ3'- GAL1$_{prom}$-YAT1-leu2Δ5'::KanMX@GAL1 3'* | Fig. 1h-i, S1f-h, S2g, 5c, S4i | Obtained by homologous recombination into YKD1683 using a cassette encompassing *leu2* repeats and the *YAT1* transgene, retrieved from pBP2057 by PacI-PmeI restriction and further integrated at *GAL1 3'*, upstream LexA-BS. |
| YPB2103 | *wt* (*intron-YAT1)* | (W303) *LacO@GAL10 3'::TRP1 his3::LacI-GFP::HIS3 LexA-BS@GAL1 3' NUP49::NUP49-mCherry-HphMX leu2Δ3'- GAL1$_{prom}$ -intron-YAT1-leu2Δ5'::KanMX@GAL1 3'* | Fig. 1i, S1f-g | Obtained by homologous recombination into YKD1683 using a cassette encompassing *leu2* repeats and the intron-containing *YAT1* transgene, retrieved from pBP2060 by PacI-PmeI restriction and further integrated at *GAL1 3'*, upstream LexA-BS. |
| YBP1501 | *tho* (BY4742) | (BY4742) *mft1::KanMX* | Fig. 2c-e, S2b, S2h-i, 3c, 4g, S4c-f, S4h, 5a, | Euroscarf |
| YBP2109 | *tho* (BY4741) | (BY4741) *mft1::KanMX* | Fig. 3d | Euroscarf |
| YPB2006 | *tho* (W303) | (W303) *mft1::KanMX* | Fig. 4d-f, S4g, 5a | The complete *MFT1* CDS was deleted by homologous recombination using a KanMX cassette amplified from pFA6a-KanMX6. |
| YKD2373 | *tho* (*HSP104)* | (YKD2204) *mft1::KanMX* | Fig. S2d, 3h, 4c | The complete *MFT1* CDS was deleted by homologous recombination using a KanMX cassette amplified from pFA6a-KanMX6. |
| YKD2564 | *nup133* (*HSP104)* | (YKD2204) *nup133::URA3* | Fig. S2e-f | The complete *NUP133* CDS was deleted by homologous recombination using a *nup133::URA3* cassette[10]. |

| | | | | |
|---|---|---|---|---|
| YBP2104 | *tho* (*GAL10*) | (YKD1683) *mft1::*NatMX | strain construction | The complete *MFT1* CDS was deleted by homologous recombination using a NatMX cassette amplified from pFA6a-NatMX6. |
| YBP2105 | *tho* (*YAT1)* | (W303) *LacO@GAL10 3'::TRP1 his3::LacI-GFP::HIS3 LexA-BS@GAL1 3' NUP49::NUP49-mCherry-HphMX leu2Δ3'-GAL1$_{prom}$-YAT1-leu2Δ5'::KanMX@GAL1 3' mft1::NatMX* | Fig. 1i, S1f-g, S2g, 5c, S4i | Obtained by homologous recombination into YBP2104 using a cassette encompassing *leu2* repeats and the *YAT1* transgene, retrieved from pBP2057 by PacI-PmeI restriction and further integrated at *GAL1 3'*, upstream LexA-BS. |
| YBP2106 | *tho* (*intron-YAT1)* | (W303) *LacO@GAL10 3'::TRP1 his3::LacI-GFP::HIS3 LexA-BS@GAL1 3' NUP49::NUP49-mCherry-HphMX leu2Δ3'- GAL1$_{prom}$ -intron-YAT1-leu2Δ5'::KanMX@GAL1 3' mft1::NatMX* | Fig. 1i, S1f-g, | Obtained by homologous recombination into YBP2104 using a cassette encompassing *leu2* repeats and the intron-containing *YAT1* transgene, retrieved from pBP2060 by PacI-PmeI restriction and further integrated at *GAL1 3'*, upstream LexA-BS. |
| YBP2307 | *NIC96-myc* | (BY4742) *NIC96-13Myc::KanMX* | Fig. 1b-d, 2d-e, S2i, 3e-f | C-terminal tagging of Nic96 was achieved through the integration of a 13Myc-KanMX cassette, amplified from pFA6a-13Myc-KanMX6, at the endogenous *NIC96* locus. Nic96-myc expression is driven by *NIC96* natural promoter. |
| YBP2308 | *tho NIC96-myc* | (BY4742) *NIC96-13Myc::KanMX mft1::NatMX* | Fig. 2d-e; S2i, 3f | The complete *MFT1* CDS was deleted by homologous recombination using a NatMX cassette amplified from pFA6a-NatMX6. |
| YBP2409 | *sac3*Δ | (W303) *sac3::KanMX* | Fig. 3b | The complete *SAC3* CDS was deleted by homologous recombination using a KanMX cassette amplified from pFA6a-KanMX6. |
| YBP2326 | *fcy1*Δ | (BY4742) *fcy1::KanMX* | strain construction | Euroscarf |
| YBP2327 | *mlh3*Δ | (BY4742) *mlh3::KanMX* | strain construction | Euroscarf |
| YBP2017 | *rad2*Δ | (BY4742) *rad2::KanMX* | strain construction | Euroscarf |
| YBP2161 | *tho* (BY4741) | (BY4741) *mft1::NatMX* | strain construction | The complete *MFT1* CDS was deleted by homologous recombination using a NatMX cassette amplified from pFA6a-NatMX6. |
| YBP2332 | *tho fcy1*Δ | (BY4742) *fcy1::KanMX mft1::NatMX* | Fig. 3c | Obtained by cross (YBP2326xYBP2161). |
| YBP2331 | *tho mlh3*Δ | (BY4742) *mlh3::KanMX mft1::NatMX* | Fig. 3c | Obtained by cross (YBP2327xYBP2161). |
| YBP2018 | *tho rad2*Δ | (BY4742) *rad2::KanMX mft1::KanMX* | Fig. 3c | Obtained by cross (YBP2017xYBP2161). |
| YBP2315 | *NIC96-myc rfa1-D228Y* | (YBP2307) *rfa1-D228Y::NatMX* | Fig. 3e-f | Obtained by homologous recombination into YBP2307 using a cassette encompassing the *RFA1* CDS carrying the D228Y mutation and the *NatMX* marker, retrieved from pBP2153 by NotI restriction and further integrated at the *RFA1 locus.* |
| YBP2319 | *tho NIC96-myc rfa1-D228Y* | (YBP2308) *rfa1-D228Y::NatMX* | Fig. 3e-f | Obtained by cross (YBP2109xYBP2315). |
| YBP1478 | *siz1*Δ *siz2*Δ | (BY4742) *siz1::KanMX siz2::KanMX* | Fig. S4c, S4e | Bretes et al.[11] |
| YBP2238 | *tho siz1*Δ *siz2*Δ | (BY4742) *siz1::KanMX siz2::KanMX mft1::NatMX* | Fig. S4c, S4e | Obtained by cross (YBP1478xYBP2161). |

| | | | | |
|---|---|---|---|---|
| YBP2277 | *slx5Δ* | (BY4742) *slx5::NatMX* | Fig. S4d | The complete *SLX5* CDS was deleted by homologous recombination using a NatMX cassette amplified from pFA6a-NatMX6. |
| YBP2237 | *tho slx5Δ* | (BY4742) *slx5::NatMX mft1::KanMX* | Fig. S4d | Obtained by cross (YBP2277xYBP2109). |
| YBP1167 | *slx8Δ* | (BY4742) *slx8::HphMX* | Fig. 4g, 5a, S4h | The complete *SLX8* CDS was deleted by homologous recombination using a HphMX cassette amplified from pFA6a-HphMX6. |
| YBP2166 | *tho slx8Δ* | (BY4742) *slx8::HphMX mft1::NatMX* | Fig. 4g, 5a, S4h | Obtained by cross (YBP1167xYBP2161). |
| YBP2324 | *rfa1-D228Y* | (BY4742) *rfa1-D228Y* | Fig. 5a, S4f | Obtained by cross (YBP2109xYBP2315). |
| YBP2325 | *tho rfa1-D228Y* | (BY4742) *rfa1-D228Y mft1::KanMX* | Fig. 5a, S4f | Obtained by cross (YBP2109xYBP2315). |
| FSY3992 | *ulp1-333* | (W303) *ULP1::HIS3 YCpLac22-ulp1-333-TRP1* | Fig. 4a, S4a-b | Infantino et al.[12] |
| Z417-17 | *rfa1-4KR* | (W303) *rfa1-* K170R, K180R, K411R, K427R *mft1::KanMX* | Fig. 4f | Dhingra et al.[13] |
| YBP2333 | *ulp1-333 rfa1-4KR* | (W303) *rfa1-* K170R, K180R, K411R, K427R; *ULP1::KanMX; YCpLac11-LEU2-ulp1-333* | Fig. 4a | The complete *ULP1* CDS was deleted by homologous recombination using a KanMX cassette (amplified from pFA6a-KanMX6) into Z417-17 cells carrying the *YCpLac11-LEU2-ulp1-333* plasmid. |
| YBP2280 | *tho rfa1-4KR* | (W303) *rfa1-* K170R, K180R, K411R, K427R *mft1::KanMX* | Fig. 4f | The complete *MFT1* CDS was deleted by homologous recombination using a KanMX cassette amplified from pFA6a-KanMX6. |
| T79-9 | *mms21-11* | (W303) *mms21-11*-LEU2 | Fig. 4d, 5a, S4g | Gift from X. Zhao |
| YBP2278 | *tho mms21-11* | (W303) *mms21-11*-LEU2 *mft1::KanMX* | Fig. 4d, 5a, S4g | Obtained by cross (T79-9x[*mft1Δ* mat a W303]). |
| YBP2282 | *smt3-3KR* | (W303) *smt3- K11R, K15R, K19R::TRP1* | Fig. 4e | Lescasse et al.[14] |
| YBP2290 | *tho smt3-3KR* | (W303) *smt3- K11R, K15R, K19R::TRP1 mft1::KanMX* | Fig. 4e | Obtained by cross (YBP2282x[*mft1Δ* mat a W303]). |
| MNY1125 | *rfa1-D228Y* | (W303) *rfa1-D228Y* | strain construction | Luciano et al.[15] |
| YKD2206 | *rfa1-D228Y* (*HSP104)* | (YKD2204) *rfa1-D228Y* | Fig. 3h | Derived from YKD2204 and MNY1125 by successive crosses. |
| YKD2338 | *tho rfa1-D228Y* (*HSP104)* | (YKD2204) *rfa1-D228Y mft1::KanMX* | Fig. 3h | The complete *MFT1* CDS was deleted by homologous recombination using a KanMX cassette amplified from pFA6a-KanMX6. |
| YKD2426 | *rfa1-4KR* (*HSP104)* | (YKD2204) *rfa1-* K170R, K180R, K411R, K427R | Fig. 4c | Derived from YKD2204 and Z417-17 by successive crosses. |
| YKD2463 | *tho rfa1-4KR* (*HSP104)* | (YKD2204) *rfa1-* K170R, K180R, K411R, K427R *mft1::KanMX* | Fig. 4c | The complete *MFT1* CDS was deleted by homologous recombination using a KanMX cassette amplified from pFA6a-KanMX6. |
| YKD2372 | *mms21-11* (*HSP104)* | (YKD2204) *mms21-11::LEU2* | Fig. 4c | Obtained from YKD2204 and T79-9 by successive crosses. |
| YKD2375 | *tho mms21-11* (*HSP104)* | (YKD2204) *mms21-11::LEU2 mft1::KanMX* | Fig. 4c | The complete *MFT1* CDS was deleted by homologous recombination using a KanMX cassette amplified from pFA6a-KanMX6. |

**Supplementary Table 3. Plasmids used in this study**.

| CODE | NAME | RELEVANT FEATURES | SOURCE | USAGE (Fig.) |
|---|---|---|---|---|
| pBP414 | *pFA6a-KanMX6* | AmpR; $TEF_{prom}$-*KanMX6*-$TEF_{term}$ | Longtine et al.[16] | Strain construction |
| pBP679 | *pFA6a-NatMX6* | AmpR; $TEF_{prom}$-*NatMX6*-$TEF_{term}$ | Hentges et al.[17] | Strain construction |
| pBP672 | *pFA6a-HphMX6* | AmpR; $TEF_{prom}$-*HphMX6*-$TEF_{term}$ | Hentges et al.[17] | Strain construction |
| pBP780 | *pFA6a-13Myc-KanMX6* | AmpR; *13Myc*-$TEF_{prom}$-*KanMX6*-$TEF_{term}$ | Longtine et al.[16] | Strain construction |
| pBP1172 | *YCpLac11-LEU2-ulp1-333* | AmpR/*LEU2/CEN; ULP1*$_{prom}$-*ulp1-333* | Bretes et al.[11] | Strain construction |
| pBP2057 | *pFA6a-YAT1 ** | AmpR; *GAL1 3'- leu2*$\Delta$*3'-pGAL1-YAT1-leu2*$\Delta$*5'::KanMX-GAL1 3'* | This Study | Strain construction |
| pBP2060 | *pFA6a-intron-YAT1 ** | AmpR; *GAL1 3'- leu2*$\Delta$*3'-pGAL1-RPL51A*intron-YAT1-leu2*$\Delta$*5'::KanMX- GAL1 3'* | This Study | Strain construction |
| pBP2153 | *pRS315-rfa1-D228Y-NatMX* | AmpR/*LEU2/CEN*; *rfa1*$_{D228Y}$-*NatMX6-RFA1 3'* | This Study | Strain construction |
| pBP2182 | *pRS315-TET-off scRNH1-Flag* | AmpR/*LEU2/CEN*; *CMV*$_{prom}$*-TetR-VP16, tetO*$_7$-*scRNH1-3xFlag* | This study | Fig. 2a; S2b |
| pBP1932 | *pRS423-GPD-hsRNH1* | AmpR/*HIS3/2µ*; *GPD*$_{prom}$*-myc-hsRNH1-CYC1*$_{term}$ | Bonnet et al.[3] | Fig. 2c, S2h-i |
| pBP1026 | *pRS316-NUP49-mCherry* | AmpR/*URA3/CEN*; *NUP49*$_{prom}$*-NUP49-mCherry* | Chadrin et al.[18] | Fig. 3h, 4c, S2d-f |
| pBP2155 | *pRS316-His*$_6$*-SMT3* | AmpR/*URA3/CEN*; *SMT3*$_{prom}$*-His6-SMT3-SMT3*$_{term}$ | This study | Fig. 4a, S4a-b |
| pBP1882 | *pBTM116-URA-LexA* | AmpR/*URA3/2µ*; *ADH1*$_{prom}$*-LexA* | Texari et al. [9] | Fig. 5c, S4i |
| pBP1883 | *pBTM116-URA-LexA-Nup60* | AmpR/*URA3/2µ*; *ADH1*$_{prom}$*-LexA-NUP60* | Texari et al. [9] | Fig. 5c, S4i |

* *YAT1* reporter cassettes encompass: (i) a 100bp DNA fragment homologous to *GAL1 3'* (133-232bp downstream *GAL1* stop codon); (ii) the *leu2*$\Delta$*3'-GAL1*$_{prom}$*-YAT1-leu2*$\Delta$*5'* or *leu2*$\Delta$*3'-GAL1*$_{prom}$*-RPL51A*intron-YAT1-leu2*$\Delta$*5'* reporter constructs, as previously defined[3]; (iii) the KanMX selection marker; (iv) a 100bp DNA fragment homologous to *GAL1 3'* (234-333bp downstream *GAL1* stop codon). Homologous recombination allows the integration of the cassette at *GAL1* 3' (233bp downstream the stop codon), upstream LexA binding sites (inserted 334bp downstream the stop codon in the FSY5216 parental strain[9]).

**Supplementary Table 4. Sequences of oligonucleotides used in this study.**

| | |
|---|---|
| ***HSP104* F** | GTTCTACCAAATCACGAAGC |
| ***HSP104* R** | TCTAGGTCATCATCAATTTCC |
| ***YEF3* F** | GATTGCCGGTGGTAAGAAGA |
| ***YEF3* R** | CGTAAGCATCACCCAATTCC |
| **Intergenic* F** | GAAACCACGAAAAGTTCACCA |
| **Intergenic* R** | AGCTTCTGCAAACCTCATTTG |
| ***YAT1* F** | TCTGTGGTGGTGTCCTCAAG |
| ***YAT1* R** | CTTGCTGCCGTTTGAAGATG |
| ***ACT1* F** | ACGTTACCCAATTGAACACG |
| ***ACT1* R** | AGAACAGGGTGTTCTTCTGG |
| ***GSY2* F** | ATGACCCCTGGTGATTTGGG |
| ***GSY2* R** | TCAGCATATGGGCCATCGTC |
| ***PAU17* F** | CCCCGCTGACCAAGTCACTA |
| ***PAU17* R** | AGCAGTGTAGATACCGTCTGC |
| ***SSA4* F** | TGGAATCCATTGCTTACTCTTTGA |
| ***SSA4* R** | AGCCTTCTTAGTGACAGCGT |

* chrIV:43199..53262

## Supplementary References


1. Pelechano, V., Chávez, S. & Pérez-Ortín, J. E. A complete set of nascent transcription rates for yeast genes. *PloS One* **5**, e15442 (2010).
2. Wahba, L., Costantino, L., Tan, F. J., Zimmer, A. & Koshland, D. S1-DRIP-seq identifies high expression and polyA tracts as major contributors to R-loop formation. *Genes Dev.* **30**, 1327–1338 (2016).
3. Bonnet, A. *et al.* Introns Protect Eukaryotic Genomes from Transcription-Associated Genetic Instability. *Mol. Cell* **67**, 608-621.e6 (2017).
4. Aiello, U. *et al.* Sen1 is a key regulator of transcription-driven conflicts. *Mol. Cell* S1097-2765(22)00604–9 (2022) doi:10.1016/j.molcel.2022.06.021.
5. Mouaikel, J. *et al.* High-frequency promoter firing links THO complex function to heavy chromatin formation. *Cell Rep.* **5**, 1082–1094 (2013).
6. Reusswig, K.-U. *et al.* Unscheduled DNA replication in G1 causes genome instability and damage signatures indicative of replication collisions. *Nat. Commun.* **13**, 7014 (2022).
7. García-Pichardo, D. *et al.* Histone Mutants Separate R Loop Formation from Genome Instability Induction. *Mol. Cell* **66**, 597-609.e5 (2017).
8. Rougemaille, M. *et al.* THO/Sub2p Functions to Coordinate 3′-End Processing with Gene-Nuclear Pore Association. *Cell* **135**, 308–321 (2008).
9. Texari, L. *et al.* The Nuclear Pore Regulates GAL1 Gene Transcription by Controlling the Localization of the SUMO Protease Ulp1. *Mol. Cell* **51**, 807–818 (2013).
10. Belgareh, N. & Doye, V. Dynamics of nuclear pore distribution in nucleoporin mutant yeast cells. *J. Cell Biol.* **136**, 747–759 (1997).
11. Bretes, H. *et al.* Sumoylation of the THO complex regulates the biogenesis of a subset of mRNPs. *Nucleic Acids Res.* **42**, 5043–5058 (2014).
12. Infantino, V. *et al.* The mRNA export adaptor Yra1 contributes to DNA double-strand break repair through its C-box domain. *PloS One* **14**, e0206336 (2019).
13. Dhingra, N., Wei, L. & Zhao, X. Replication protein A (RPA) sumoylation positively influences the DNA damage checkpoint response in yeast. *J. Biol. Chem.* **294**, 2690–2699 (2019).

14. Lescasse, R., Pobiega, S., Callebaut, I. & Marcand, S. End-joining inhibition at telomeres requires the translocase and polySUMO-dependent ubiquitin ligase Uls1. *EMBO J.* **32**, 805–815 (2013).
15. Luciano, P. *et al.* RPA facilitates telomerase activity at chromosome ends in budding and fission yeasts. *EMBO J.* **31**, 2034–2046 (2012).
16. Longtine, M. S. *et al.* Additional modules for versatile and economical PCR-based gene deletion and modification in Saccharomyces cerevisiae. *Yeast Chichester Engl.* **14**, 953–961 (1998).
17. Hentges, P., Van Driessche, B., Tafforeau, L., Vandenhaute, J. & Carr, A. M. Three novel antibiotic marker cassettes for gene disruption and marker switching in Schizosaccharomyces pombe. *Yeast Chichester Engl.* **22**, 1013–1019 (2005).
18. Chadrin, A. *et al.* Pom33, a novel transmembrane nucleoporin required for proper nuclear pore complex distribution. *J. Cell Biol.* **189**, 795–811 (2010).